AIAA JOURNAL
Vol. 36, No. 3, March 1998

Study of the Unsteady Flow Features on a Stalled Wing

Steven A. Yon* and Joseph Katz†
San Diego State University, San Diego, California 92182

The occurrence of large-scale structures in the poststall flow over a rectangular wing at high angles of attack was investigated in a small-scale subsonic wind tunnel. Mean and time-dependent measurements within the separated flowfield suggest the existence of two distinct angle-of-attack regimes beyond wing stall. The shallow stall regime occurs over a narrow range of incidence angles (2–3 deg) immediately following the inception of leading-edge separation. In this regime, the principal mean flow structures, termed stall cells, are manifested as a distinct spanwise periodicity in the chordwise extent of the separated region on the model surface with possible lateral mobility not previously reported. Within the stall cells and on the wing surface, large-amplitude pressure fluctuations occur with a frequency much lower than anticipated for bluff body shedding and with minimum effect in the far wake. In the deep stall regime, stall cells are not observed, and the separated region near the model is relatively free of large-amplitude pressure disturbances.

Nomenclature

AR = span/chord, aspect ratio
C_D = drag coefficient, drag/$(\frac{1}{2}\rho V_\infty^2 S)$
C_L = lift coefficient, lift/$(\frac{1}{2}\rho V_\infty^2 S)$
C_p = pressure coefficient, $p - p_\infty/(\frac{1}{2}\rho V_\infty^2)$
c = wing chord
l = frontal projected height, e.g., $c \sin\alpha$
Re = Reynolds number, $\rho V_\infty c/\mu$
S = wing area
Sr = Strouhal number, $\omega l/V_\infty$
V_∞ = air velocity
α = angle of attack
μ = air viscosity
ρ = air density
ω = frequency

Introduction

THE transition from an attached flowfield over a wing into a time-dependent, partially separated flow is still not completely understood in spite of its importance to many disciplines where high lift is necessary. In addition to possible benefits from increasing the lift of wings beyond their stall angle, the understanding of such flows can reduce airframe noise, delay structural failure due to fatigue and flutter, or even improve airplane safety in conditions such as stall/spin. Most experimental investigations with stalled wings, e.g., Ref. 1, document the time-dependent nature of the separated flow, often with clearly structured vortex shedding patterns. However, even when a two-dimensional approach is taken, the von-Kármán-type vortex-shedding model with its unique frequency ($Sr \approx 0.15$) is not the only pattern observed. In fact, a large body of evidence suggests that the fluctuations associated with stall flutter occur at much lower Strouhal numbers, in the range $0.02 < Sr < 0.05$ (Refs. 1–3). Zaman et al.,[4] in their two-dimensional investigation, found these low-frequency fluctuations to occur within a narrow range of incidence angles beginning just after the onset of separation, near the point of maximum lift. Zaman et al.[4] and, earlier, Moss[5] both suggest that the low-frequency phenomena are related to a periodic stall/unstall mechanism. During three-dimensional flow visualization experiments with high-aspect ratio wings, past the point of stall, a periodic spanwise cellular pattern was observed,[6,7] with narrow attached flow regions between the separated cells. The regions of separated flow, termed stall cells, appear along the wing span with the number of cells determined by aspect ratio. Initial efforts to explain the periodicity of those stall cells led Weihs and Katz[8] to formulate a model for stall cell formation based on a Crow[9]-type instability of spanwise vortices formed by the separated leading-edge shear layer.

When one combines the experimental information gathered by the two- and three-dimensional experiments, several questions arise, particularly regarding the relation between the periodic wake shedding and the spanwise cellular patterns, as well as how and whether the two fundamental frequencies relate to each other and what effect the resulting flow structures have on the pressure fluctuations on the wing surface and the lift. The objective of the present study, therefore, is to provide additional information on the three-dimensional, time-dependent flow near the stalled wing and in its wake in terms of flow visualization and pressure measurements so that some of the preceding questions may be addressed.

Method of Investigation

The wind tunnel used in the current experiment is a subsonic, closed circuit, vertical return facility with a 0.81×1.14 m (32×45 in.) atmospheric pressure test section, with turbulence levels on the order of 1% (in the test section). Because of this turbulence level, combined with the roughness of the leading edge and the shape of the pressure distribution near stall condition, it was assumed that the flow on the suction side of the wing and the emanating shear layers are turbulent. The experiments focused on measuring the aerodynamic loads, the surface pressures, and their time-dependent fluctuations and on surface flow visualizations. A schematic description of the wing, as mounted in the wind tunnel, is shown in Fig. 1a. The wing model employed in the experiment consists of six spanwise segments, each of unit aspect ratio and 0.152 m (6 in.) chord. A photograph of one segment is shown in Fig. 1b. These segments may be combined to form a constant chord unswept wing with aspect ratio variable in integer increments from $AR = 2$ to 6. Each segment incorporates the NACA 0015 symmetric airfoil section to facilitate investigation of upper/lower surface phenomena. The addition of 0.279 m (11 in.) square tip plates allows the development of upper surface flow features with reduced influence from tip vortices. (One tip plate is shown in Fig. 1a.) Model incidence angle is variable between 0 and ±28 deg, and maximum blockage (at maximum incidence) is approximately 7%. All the results presented in this paper correspond to a Reynolds number of 6.2×10^5 (at a freestream speed of 62.6 m/s ≈ 140 mph). One surface of each of the model segments is tufted for flow visualization (Fig. 1b). Tuft orientations are photographed through the clear roof of the test section

Received April 8, 1997; presented as Paper 97-1927 at the AIAA 28th Fluid Dynamics Conference, Snowmass Village, CO, June 29–July 2, 1997; revision received Sept. 1, 1997; accepted for publication Oct. 21, 1997.

*Graduate Student, Department of Aerospace Engineering and Engineering Mechanics; currently Research Associate, Department of Applied Mechanics and Engineering Science, University of California, San Diego, La Jolla, CA 92093. Member AIAA.

†Professor, Department of Aerospace Engineering and Engineering Mechanics. Associate Fellow AIAA.

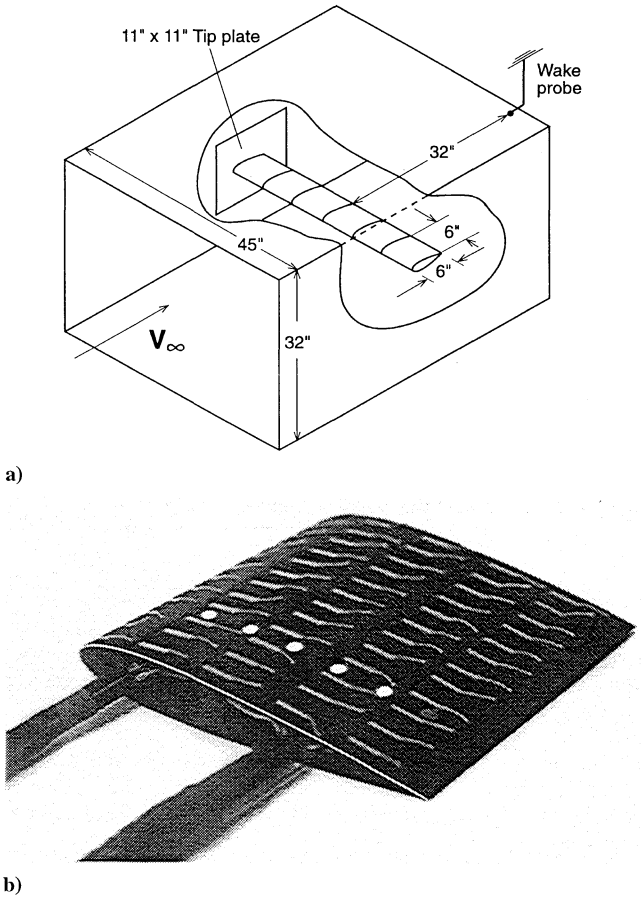

Fig. 1 a) Layout of the rectangular wing in the wind-tunnel test section and b) the instrumented model segment showing surface tufts and pressure transducers. The wiring and static pressure tubes are contained entirely within the model and exit through the tip.

to provide a record of the surface flow averaged over the length of the exposure. Time-dependent behavior of the tufts is recorded on VHS tape with an oblique view down the span of the model.

One of the model segments is instrumented for mean and high-frequency static pressure measurements. Five static pressure ports and five Endevco piezo-resistive static pressure transducers are arranged in a chordwise array approximately 0.038 m ($1\frac{1}{2}$ in.) from the edge of the model segment as shown in Fig. 1b (see five small circles). The transducers respond to absolute pressure from 0 to 1.02 atm (0–15 psi) with a resolution of 1.7×10^{-5} atm (0.00025 psi) and a maximum frequency response greater than 150,000 Hz. The small size of the active area (less than 3 mm^2 or 0.005 $in.^2$) allows examination of relatively fine-scale structure in the unsteady pressure field. The pressure field characteristic of various regions of the separated flow, e.g., within the separation cells, is obtained by moving the instrumented segment to the appropriate spanwise location on the model. A single transducer mounted on a vertical streamlined strut 0.81 m (32 in.) downstream of the trailing edge serves as a wake pressure probe (see Fig. 1a).

Each of the five pressure transducers is dc coupled to a signal conditioner through doubly shielded wires to minimize static noise and crosstalk. Typical signal-to-noise ratios are on the order of 100–1000, and the minimum pressure fluctuation that can be resolved is on the order of the noise in the signal (approximately 1.7×10^{-5} atm or 0.00025 psi). Transducer output voltages are acquired with a timed sweep through the transducer array resulting in a Nyquist frequency of 7.5 kHz in each channel. The resulting data set contains six sequences of digitally sampled transducer output voltage data, each consisting of 4400 samples spanning 0.293 s. Although the sweep rate employed in this experiment is substantially higher than the frequency of any anticipated natural pressure fluctuation, it is necessary for the resolution of any distinct waveforms in the pressure histories. Application of fast Fourier transform, autocorrelation, and cross-correlation algorithms were used for the analysis of the resulting pressure histories in time and frequency space. A complete description of the data reduction procedures is given in Ref. 10.

Flow Visualization, Average Pressures, and Loads

The mean surface features associated with the separated flowfield are visualized with an array of fine tufts on the upper surface of the model. These tufts are free to respond to transient flowfield events and thus may also give some indication of the unsteady characteristics of the flow. During the experiment, the model angle of attack was increased until the onset of stall and the cellular separation patterns formed. The stall cell phenomenon is observed in the present results in a narrow angle-of-attack range, spanning 2 or 3 deg at most, beginning around 17-deg angle of attack. A typical two-cell pattern observed in the present experiment is shown in Fig. 2a, which is an enhanced photograph of the upper surface of an aspect ratio 6 model at 17 deg. Next a schematic of the key features of the surface flowfield are presented. Each cell is defined by the line of separation that displays the characteristic owl's eye pattern reported by Winkelmann and Barlow.[7] Within the stall cells, rapid movements of the tufts indicate a largely unsteady environment, whereas outside of the cells, very little tuft motion is noted. The region of attached flow between adjacent cells extends to the midchord, whereas downstream of this point, tuft motion indicates increased unsteadiness and possibly separation near the trailing edge.

The mean direction of the surface flow adjacent to the cell boundaries is indicated by the arrows in Fig. 2b. The circulation around the lateral cell boundaries, implied by the variation of the surface velocity within and external to the individual cells, is consistent with the presence of spiral nodes terminating the line of separation on the wing surface, as noted by Winkelmann and Barlow,[7] although these nodes are not directly observed in the present results. The direction of the near surface flow in and around the separation cells has implications for the orientation of the vorticity vector in the separated shear layer. Near the centerline of each cell, where the spanwise velocity component is absent, the vorticity vector on the model surface (along the line of separation) must point in the spanwise direction. On either side of the centerline of the cell, however, in association with the spanwise velocity components near the model surface, the vorticity vector must have a significant streamwise component. The sense of the streamwise vorticity in the shear layer on either side of the cell is consistent with the circulation around the spiral nodes inferred to exist at the lateral boundaries of the line of separation, i.e., both lateral edges induce an upward velocity component at the centerline of the cell. The lateral edges of each shear layer may therefore be bounded by a zone of streamwise vorticity, which rolls up into vortex cores that join the wing surface at the location of the spiral nodes. Winkelmann and Barlow[7] suggest that these vortices

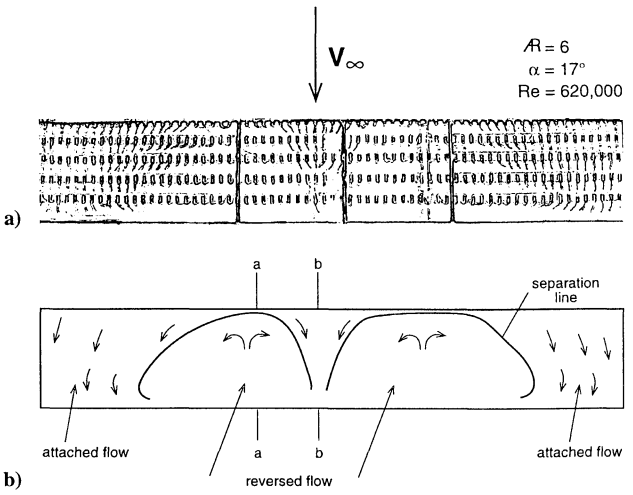

Fig. 2 a) Enhanced photograph of tuft orientations showing a stable two-cell separation pattern on the aspect ratio 6 model and b) schematic outline indicating the approximate location of the line of separation (cell boundary). Sections a–a and b–b mark the locations of the transducer and static pressure arrays, relative to the stall cell boundaries, during data acquisition.

are connected across the cell in a coherent spanwise vortex. The actual location of the vortex cores away from the model surface is not indicated by the surface flow visualization but may be inferred from the mean surface pressure distribution, to be discussed subsequently.

When more than one cell is observed on the wing surface, e.g., the two-cell pattern shown in Fig. 2, each cell exhibits an irregular dynamic motion best described as jostling. Slight lateral movements of any cell result in a corresponding adjustment in the adjacent cells. These movements seem to be arbitrary and may be slight or vigorous, and in the latter case one of the cells may momentarily merge with another. The unsteady nature of the separation cells becomes apparent only through the use of visualization techniques, which respond on timescales on the order of the unsteady motions, e.g., small surface tufts. The surface oil technique employed by Gregory et al.[6] and Winkelmann and Barlow[7] has a relatively long response time, so that this motion had not been previously reported. A distinct frequency for the lateral motion of the cells was not observed.

The number of discrete cells observed in the separated flowfield above the incipiently stalled wing depends on the wing aspect ratio, as noted by Winkelmann and Barlow,[7] and the dependence is summarized in Fig. 3. The tip plates employed in the present experiment allow the formation of a larger number of cells on a model of fixed aspect ratio, and the net effect is seen to be a displacement in the ordinate of the best fit line from the experimental data of Winkelmann and Barlow.[7] In both cases, each stable cell is observed to occupy a region approximately two chords in width. The lateral extent of a cell is essentially independent of the number of cells observed and appears to be controlled by a chordwise length scale. Models exhibiting one-, two-, or three-cell patterns all produce cells of approximately the same width.

The stability of a given separation pattern (number of cells) on a model of fixed aspect ratio is defined by the relative amount of time over which that pattern is observed. A stable pattern is therefore one that is observed almost exclusively. Unstable patterns result when the model aspect ratio is intermediate between two values for which stable patterns are observed. In Fig. 3, models of aspect ratio between 3.5 and 4.5 produce two-cell patterns that are stable. Increasing the aspect ratio to 5.0–6.0 results in an unstable switching between two- and three-cell patterns. The essential difference between a stable pattern and an unstable pattern appears to be the width of the attached region between adjacent cells. If this region is either too wide or too narrow (the preferred width seems to be on the order of half the cell width), then adjustment occurs by the formation or destruction of a cell.

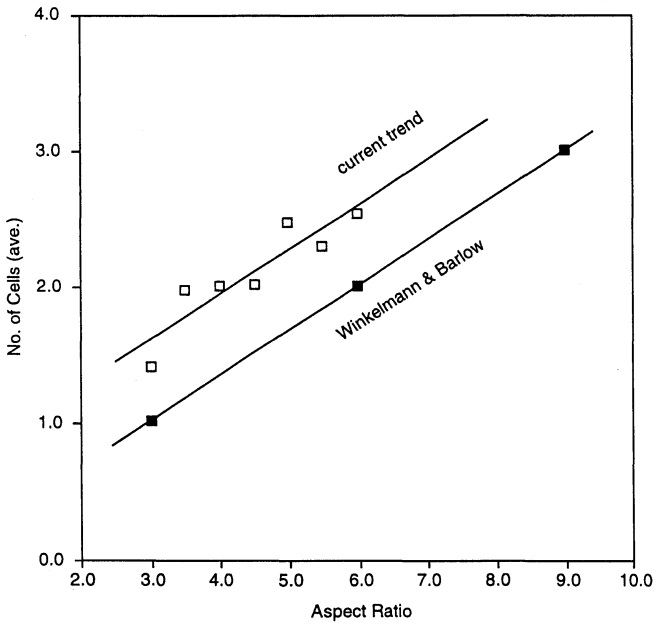

Fig. 3 Number of observed cells as a function of wing aspect ratio obtained with tip plates (□) and without tip plates (■, from Ref. 7). Noninteger numbers of cells indicate unstable switching between two integer cell patterns, e.g., 2.5 cells indicate switching between two- and three-cell patterns with equal amounts of time in each pattern.

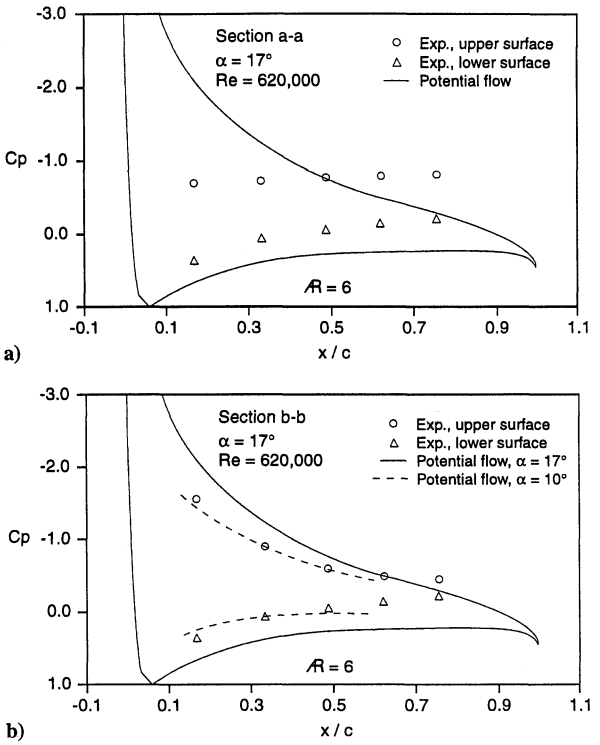

Fig. 4 a) Mean static pressure recorded within a separation cell, corresponding to section a–a in Fig. 2: ——, the three-dimensional potential solution. b) Mean static pressure recorded in the attached region between two cells, corresponding to section b–b in Fig. 2: ——, the three-dimensional potential solution at 17-deg angle of attack and – – –, the potential solution at a reduced angle of attack (10 deg).

Surface pressure measurements within the partially separated flow consisted of separate time-average and time-dependent recordings. The mean static pressure within the separation cells (section a–a in Fig. 2b) and in the intervening attached regions (section b–b in Fig. 2b) is shown in Fig. 4. For comparison, the ideal (attached) flow solution for the same geometry (indicated by the solid line) is computed with a three-dimensional potential-flow code, e.g., see Chap. 11 of Ref. 11. Within the separation cells (Fig. 4a), the mean static pressure is essentially constant, and the separated flow extends to the region of the leading edge, in agreement with the flow visualization. Mean pressure on the lower surface of the model, however, only vaguely resembles the potential-flow prediction. In the medial attached regions (Fig. 4b), mean static pressure on the upper surface deviates from the potential prediction over the entire section but appears to be consistent with an attached flow at a reduced angle of attack over the forward half of the section. The dashed lines represent the potential solution at 10-deg angle of attack to illustrate this downwash effect from the adjacent stall cells. Away from the wing tips, the source of the downwash resulting in this reduced angle of attack is not immediately apparent. Toward the trailing edge, the pressure in the medial attached region on the upper surface is essentially constant, which is consistent with separated flow and in agreement with the flow visualization.

Previous investigators have postulated the existence of a coherent spanwise vortex core spanning each stall cell and connecting the spiral nodes that terminate the line of separation bounding the cell.[7] The net effect of a spanwise vortex would be an induced upwash across the entire span of the model, which is not consistent with the increased downwash in the medial attached regions suggested by the mean pressure distribution, as shown in Fig. 4. If, instead, the vortices that join the model surface at the location of the spiral nodes trail downstream (see the normal vortex in Fig. 5), then the net effect would be an induced upwash within the cell and a downwash in the medial attached regions, which would then see an effectively smaller angle of attack. To summarize the results of the flow visualization, a schematic description of the observed mean flowfield is shown in Fig. 5. In addition to consistency with the observed pressure distribution, this model is consistent with the cell motion and stability

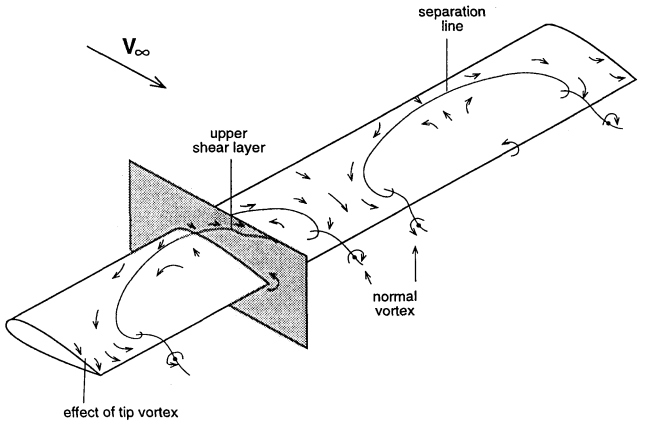

Fig. 5 Schematic model for the observed mean flowfield associated with the cellular separation. The shear layers originating on the line of separation are bounded by normal vortex cores, which trail downstream. Trailing-edge vorticity and wing tip vortices have been neglected for clarity.

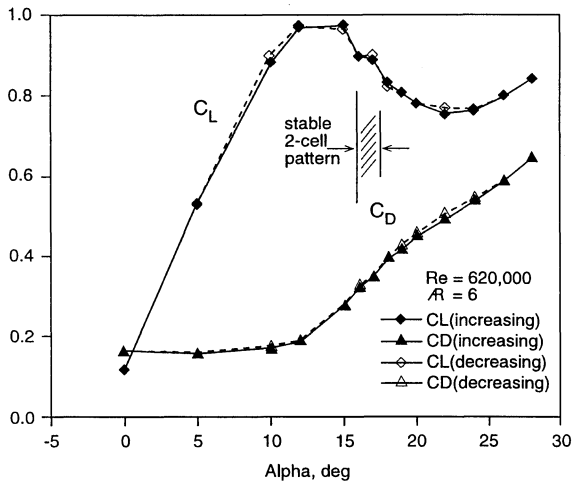

Fig. 6 Variation of mean lift and drag coefficients with increasing and decreasing angle of attack for the aspect ratio 6 model.

observed in the present experiment. If the size of the cells is fixed (through some other mechanism), then increasing the aspect ratio from that resulting in a stable separation cell pattern will result in increasing the size of the medial attached regions, which remain attached because of the downwash induced by the adjacent cells. At some critical aspect ratio, the downwash induced on the expanded medial attached regions will no longer be sufficient, and another separation cell will form. Alternately, if the aspect ratio is reduced, the cells are forced together, and one will eventually be destroyed by the induced downwash from its nearest neighbors. Similarly, random lateral motions of a cell will result in changing the distribution of induced downwash, which forces a corresponding adjustment of the positions of the remaining cells.

The effect of the stall cell separation on model lift can be deduced from the experimental data shown in Fig. 6 for an aspect ratio 6 model that experiences stable two cell separation. The data points represent a typical α sweep, with increasing and decreasing angles of attack. The finite lift at zero incidence is attributed to an error of approximately 1 deg in the angle-of-attack calibration. The hysteresis in the range where the stall cells appear ($\alpha = 17$–19 deg) is marginal. The cellular separation pattern develops a few degrees after the point of maximum lift ($C_{L\,\max}$) and the onset of separation at the trailing edge. This condition is reflected in a minor reduction in the rate of lift loss with increasing angle of attack in addition to a reduction in the variance of the measured lift coefficient compared with that measured at higher and lower incidence angles. The qualitative effects of the separation cells on the drag coefficient are similar but are slightly smaller in magnitude. The result is that although no significant gains in lift/drag ratio are realized at the optimal separation cell incidence angle, the effect of the developing separation pattern is to reduce the severity of stall by broadening the angle-of-attack range over which the stall occurs.

Unsteady Pressure

Time-dependent static pressure measurements are obtained by positioning the instrumented model segment such that the transducer and static tap arrays sample the desired region of the separated flowfield. For brevity, most of the pressure data presented here correspond to the aspect ratio 3 model. Similar data from higher aspect ratio models can be found in Ref. 10. Pressure histories typical of those observed near the trailing edge (upper surface) are shown in the inset to Fig. 7. The $\alpha = 10$ deg trace was obtained in an attached flow condition and serves as a reference signal, whereas the remaining two were obtained in the separated region near the center of the aspect ratio 3 model. Note that the largest fluctuations occur at the beginning of the range over which stall cells are observed, i.e., 17–19 deg, and that relatively small changes in model incidence can result in large changes in the character of the signal. Analysis of the separated flow pressure histories indicates that low-frequency ($Sr < 0.15$) fluctuations similar to those reported by Zaman et al.[4] occur in the separated region in association with the stall cells described in the previous section.

The amplitude and frequency content of the pressure fluctuations recorded within the separated region on a model that exhibits cellular separation are summarized in Figs. 7 and 8, respectively. The amplitude of the fluctuating pressure is defined in the inset to Fig. 7. The largest pressure fluctuations, represented by the upper series of points in Fig. 7, exhibit significant streamwise growth along the wing section and occur in association with separation cells at 17-deg angle of attack. These fluctuations occur in two distinct frequency ranges (labeled fan triggered and natural in Fig. 8), both of which correspond to Strouhal numbers less than that associated with bluff body shedding ($Sr < 0.15$). Outside of the narrow range of incidence angles associated with cellular separation, the amplitude of the measured surface pressure fluctuations is much less, and the low-frequency signal is absent. These observations suggest division of the range of orientations examined into two regimes—shallow stall (where cellular separation is observed) and deep stall—which are discussed in detail next.

The shallow stall regime is characterized by the appearance, 2 or 3 deg after the first indications of separation at the trailing edge of the model, of separation cells in the upper surface flowfield and large-amplitude, low-frequency static pressure fluctuations within the separated flow on the model surface. Examples of pressure histories from all five surface pressure transducers, recorded near the centerline of a separation cell at 17-deg angle of attack, are shown together in Fig. 9, in which the pressure histories are presented sequentially

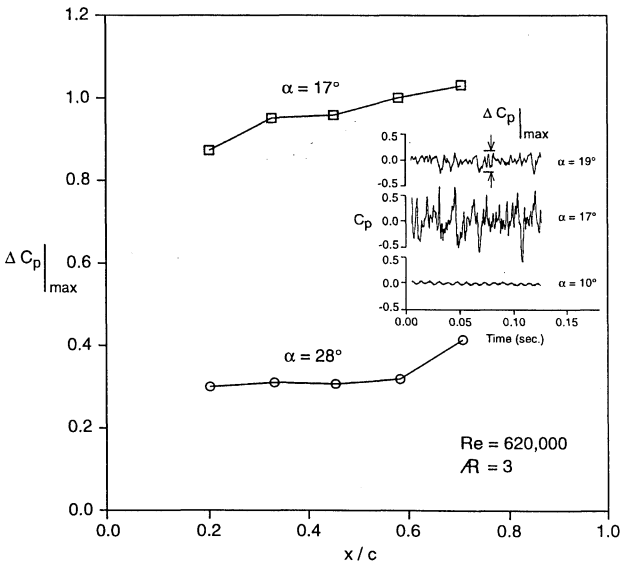

Fig. 7 Maximum amplitude of static pressure fluctuations within a stall cell at 17-deg angle of attack (upper curve) and in the separated region at 28-deg angle of attack (lower curve).

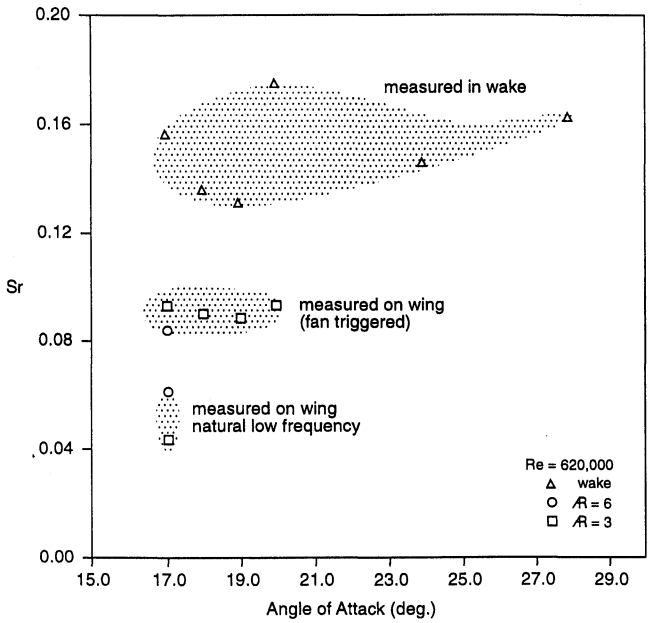

Fig. 8 Variation of the Strouhal number associated with pressure fluctuations in the wake and on the model surface as a function of angle of attack.

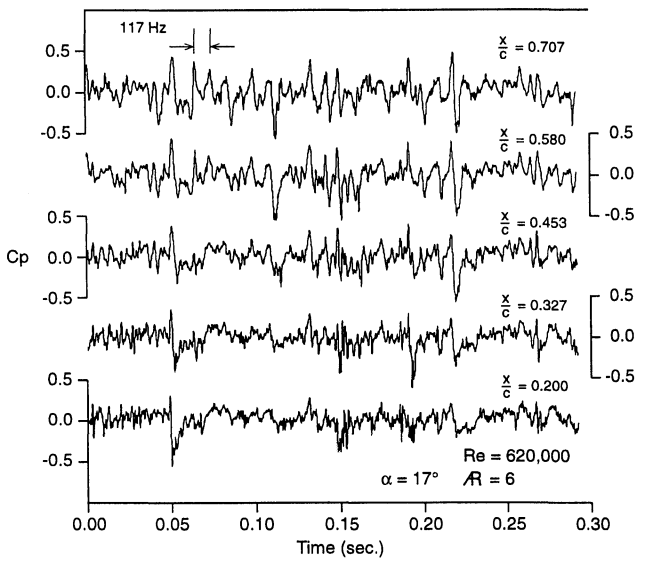

Fig. 9 Time histories of pressure coefficient associated with forced low-frequency fluctuations within a stall cell. These are to be viewed as fluctuations around the mean of each signal. The transducers are numbered sequentially from the leading edge (lowest), and the chordwise location of each transducer is indicated to the right. The period of the 117-Hz component is indicated in the topmost trace.

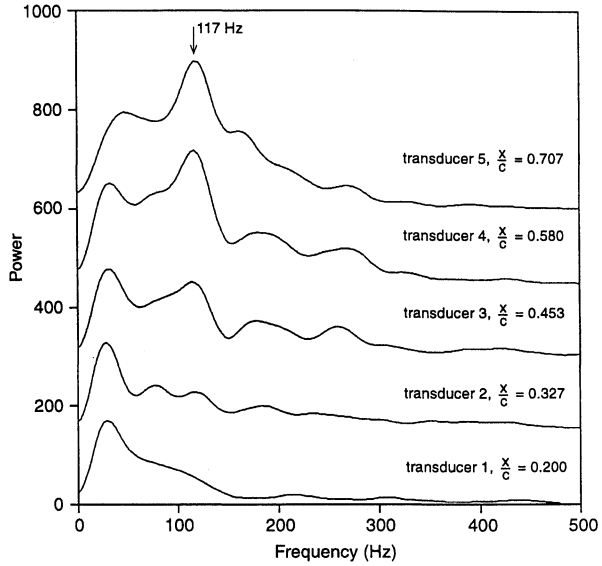

Fig. 10 PSD estimators computed from the time histories in Fig. 9. The chordwise location of each transducer is indicated to the right. Successive spectra are vertically offset by 150 units for clarity. Power associated with strong 117-Hz component is indicated by the arrow at the top.

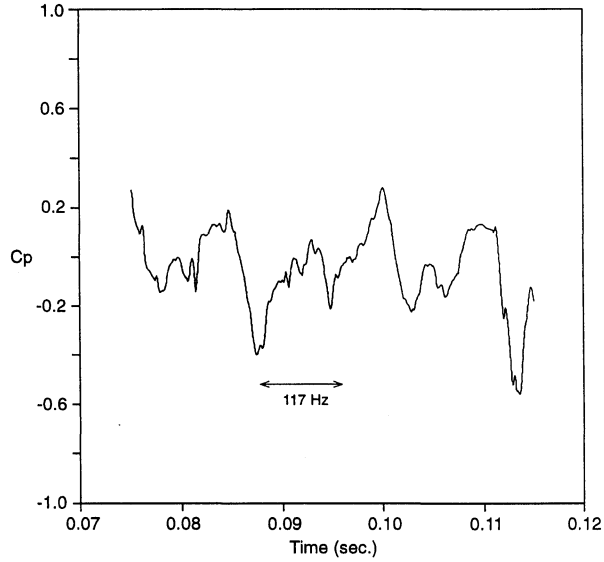

Fig. 11 Waveform associated with the forced 117-Hz pressure fluctuations. The period is indicated for reference. This waveform is clearly visible only in the records from the aft most transducer (x/c = 0.707).

from the leading edge, with the leading-edge record at the bottom. Over the duration of the pressure data acquisition, the fluctuations appear to be stationary. The largest pressure fluctuations can be visually identified in each of the five transducer records, and when measured, they generally exhibit significant streamwise growth. The pressure fluctuations characteristic of the shallow stall regime occur, with decreasing amplitude at higher incidence angles, up to 19- or 20-deg angle of attack.

The frequency space representations of the stall cell pressure histories are shown in Fig. 10. The power spectral density (PSD) estimators in Fig. 10 are presented sequentially from the leading edge, with the leading edge at the bottom. The significant low-frequency power (<50 Hz) is attributable to tunnel vibration (near the fan rotational frequency) and is not considered. The greatest streamwise growth in any frequency range occurs around 117 Hz, which is the blade pass frequency of the fan drive. Peak power occurs at this frequency in the record from the trailing-edge transducer, and the streamwise growth of the large pressure fluctuations recorded during stall cell separation is attributed to increased power near this frequency. The strong 117-Hz fluctuations in the pressure histories recorded within the separation cells occur at a Strouhal number of approximately 0.08–0.10, represented by the shaded region labeled fan triggered in Fig. 8. Note that although this range is significantly lower than the value expected for vortex shedding from a bluff body (~0.15), it is still higher than the value of ~0.02 obtained by Zaman et al.[4]

A distinct waveform corresponding to the 117-Hz periodicity identified in the pressure histories recorded within the separation cells is shown in Fig. 11. The waveform is characterized by a period of gradually increasing pressure followed by a more rapid reduction in pressure and is readily apparent only in the record from the trailing-edge transducer, even though significant power at this frequency occurs over much of the section chord.

Cross correlations of the leading-edge pressure record in Fig. 9 with the downstream pressure histories are shown in Fig. 12. The transducers involved in each case are indicated above the corresponding curve. Cross correlation between any two adjacent transducers in the stall cell pressure histories results in peak coefficients

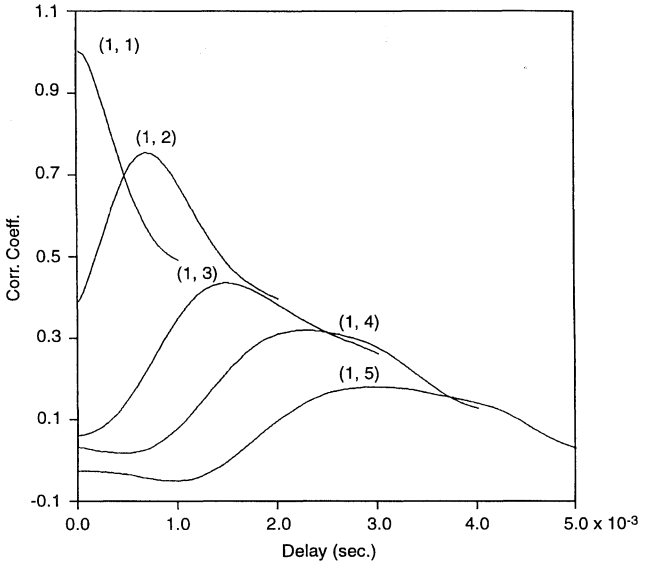

Fig. 12 Correlation coefficients between pairs of pressure histories in Fig. 9, with the transducer pairs indicated in parentheses.

greater than 0.7 and convective speeds, based on the delay to peak correlation and the streamwise separation of the transducers, of approximately half the freestream speed. Although the peak correlation coefficient decreases with increasing distance between the two transducers, the computed convective speed is always close to half the freestream. Length scales computed from the autocorrelation of each pressure record in Fig. 9 are on the order of the size of the transducer array (0.076 m or 3 in.), which suggests that the leading-edge shear layer did not roll up into a discrete spanwise vortex core in the vicinity of the model.

The pressure histories shown in Fig. 9 are representative of one of two types containing large-amplitude, low-frequency fluctuations that are observed within the separation cells. Both types exhibit significant streamwise growth of the lower frequency components and convection with approximately half the freestream speed, whereas the two types differ primarily in the frequency associated with the largest amplitude fluctuations. Peak power in the most commonly observed type, represented by the pressure histories in Fig. 9, occurs near 117 Hz, the blade pass frequency of the fan drive. In the remaining type, which is much less frequently observed and occurs in a much narrower range of incidence angles, peak power occurs in a lower frequency range (near 75 Hz), corresponding to Strouhal numbers represented by the shaded region labeled natural in Fig. 8. This range of Strouhal numbers (~0.04) is much closer to the value obtained by Zaman et al.[4] Previous studies have shown that wake instabilities are susceptible to forcing at frequencies higher than the naturally occurring ones.[12] In the present study, the ambient power in the test section, i.e., at the blade pass frequency of the fan drive, serves as the forcing function. The similarity of the essential features of the two types of fluctuations observed in the present study and the relative frequency of observation are consistent with the identification of the two as the natural and forced forms of the same phenomenon. The higher frequency (~117 Hz) more commonly observed fluctuations are therefore postulated to result from forcing the lower frequency (~75 Hz) natural fluctuations.

In addition to the natural and forced fluctuations just described, a third type of pressure history is also observed within the stall cells. Over significant time intervals (>0.3 s) the pressure fluctuations within the cells may be quite small and without substantial power in either of the frequency ranges associated with the large-amplitude signals described earlier. These periods of quiet separation suggest that the large-amplitude, low-frequency fluctuations are not causally related to the cellular separation patterns because the mean features of the flowfield, i.e., the stall cells, are independent of the type of pressure fluctuations recorded on the model surface.

Increasing the model angle of attack substantially beyond the optimal separation cell orientation results in loss of the cellular separation, loss of the large-amplitude, low-frequency fluctuations observed within the separation cells, and reduced amplitude of all pressure fluctuations within the separated region. Samples of pressure histories representative of this deep stall regime are shown in Fig. 13. Comparison of Fig. 9 with Fig. 13 clearly shows the loss of the large amplitude. Also by identifying a particular distinct fluctuation pattern on each of these figures, the streamwise variation can be observed by following this pattern on the five chordwise recordings. Although the streamwise growth is easily identified in Fig. 9, very little such streamwise growth seems to occur in Fig. 13. PSD estimators computed from the deep stall pressure histories are essentially featureless over the frequency range characterized by maximum streamwise growth and large power in the shallow stall data and bear an increased resemblance to the ambient signature of the test section environment, represented by the $\alpha = 10$ deg trace in the inset to Fig. 7.

Wake pressure fluctuations recorded in the shallow and deep stall regimes are shown in Fig. 14, and the corresponding PSD estimators are shown in Fig. 15. Although the amplitude of the pressure fluctuations recorded by the wing-mounted transducers is a strong function of model angle of attack, the amplitude of pressure fluctuations within the wake is less variable. Between 17 and 28 deg, the magnitude of pressure fluctuations encountered in the wake is nearly constant, but the dominant frequencies are not. Near the optimal

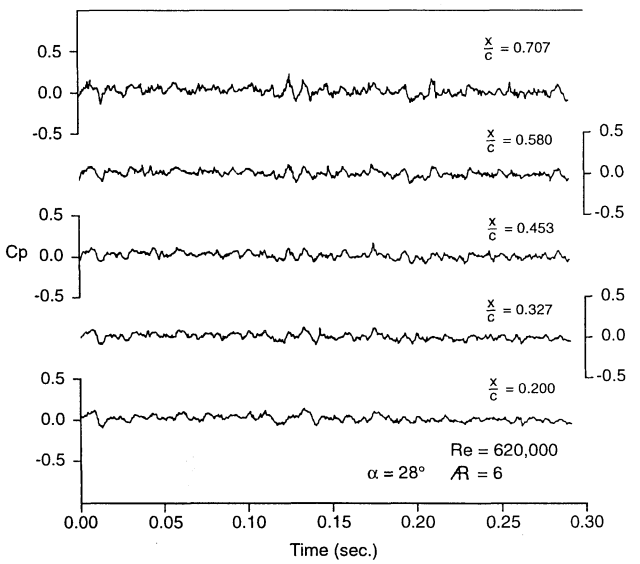

Fig. 13 Time histories of pressure coefficient recorded within the separated region at 28-deg angle of attack.

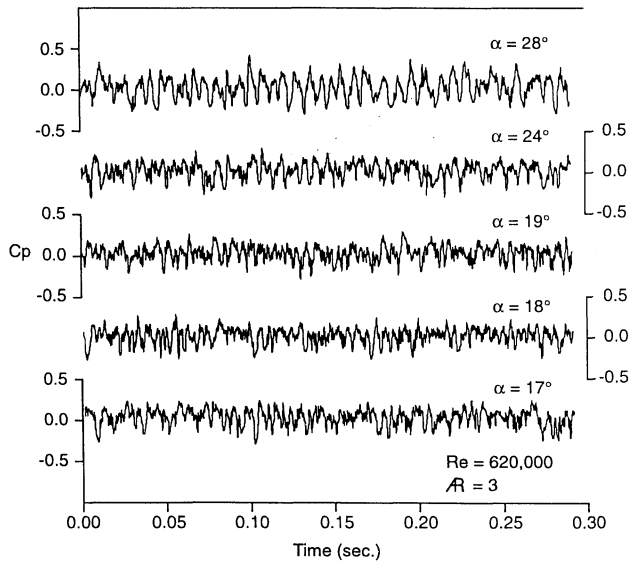

Fig. 14 Wake pressure fluctuations recorded 32 in. downstream of the trailing edge. The 17- and 18-deg data were recorded at a spanwise location behind the center of a stall cell.

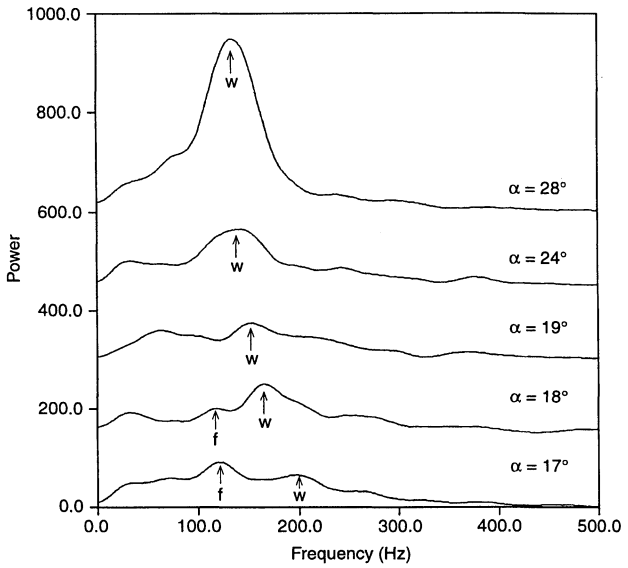

Fig. 15 PSD estimators computed from the wake pressure histories in Fig. 14 (successive spectra offset vertically by 150 units on power axis); f indicates the frequency associated with the forced fluctuations in the vicinity of the model, and w indicates power associated with von Kármán wake fluctuations.

separation cell angle of attack (~17 deg), the PSD estimators obtained from the wake fluctuations contain peaks corresponding to both the forced frequency identified within the separation cells on the model surface (~117 Hz and labeled f in Fig. 15) and a higher frequency (labeled w in Fig. 15). Power at the forced frequency is significantly reduced from that noted in the model surface pressure histories. At higher angles of attack, the forced frequency vanishes, whereas the remaining peak (w) occurs at reduced frequencies. Comparison with Fig. 8 shows that this wake frequency occurs with a Strouhal number, $Sr \sim 0.15$, corresponding to the expected bluff body vortex-shedding frequency at all model orientations. Although power at the forced frequency may result from convection and decay of the structures responsible for the large-amplitude fluctuations in the vicinity of the model, power at the higher frequency (w) was not noted in the PSD estimators from the surface pressure data and must result from formation of coherent structures in the evolving wake. Because the wake frequency is higher than the dominant model surface frequency, vortex pairing in the wake does not explain the observed behavior. Cimbala et al.[13] have reported similar wake structures resulting from instability in the evolving wake profile downstream of a decaying von Kármán vortex street.

The streamwise growth of the low-frequency fluctuations observed in the shallow stall regime on the upper surface of the model, combined with the measured convective speed approximately equal to half the freestream speed, suggests that the large-amplitude fluctuations in the vicinity of the model are related to a convective instability in the leading- and trailing-edge shear layers bounding the separation cells. Over the model transducer array, the length scale associated with the largest pressure fluctuations is larger than would be expected from convecting coherent vortex cores close to the model surface, so that the surface pressure fluctuations within the separation cells are not simply the reflection of a reduced frequency von Kármán vortex street in the vicinity of the model. Zaman et al.[4] observed a violent motion of the leading-edge shear layer termed shear layer flapping, in association with the low-frequency fluctuations. A convecting instability of the leading-edge shear layer might be described as flapping, particularly if the line of separation was fixed near the leading edge, as noted in the present results. Although the flow visualization of Zaman et al.[4] is inconclusive, the flapping shear layer does not appear to deform into discrete spanwise vortex structures, consistent with the results of the present study. Zaman et al.[4] concluded that the low-frequency fluctuations connected with the observed shear layer motions resulted from a turbulent or transitional state of the separated shear layer. Although the state of the shear layer in the present experiment was not measured, the relatively high ambient turbulence in the test section, combined with the rough surface of the model (due to the presence of the tuft strips), suggests that the shear layer was turbulent, and therefore the conclusion of Zaman et al. is consistent with this experiment.

The apparent absence of concentrated spanwise vortex structures from the unsteady separated flow within separation cells and the lack of an obvious cause/effect relationship between the cells and the low-frequency pressure fluctuations, which are connected with large-amplitude shear layer motions noted in previous efforts and inferred in the present study, leave the source of the cellular separation patterns in question. There are several indications that cellular separation, although independent of the low-frequency phenomenon, is also connected with a turbulent or transitional state of the separated shear layer. First, low-Reynolds-number ($<1.5 \times 10^4$) water-tunnel visualization[14] using an aspect ratio 3 half-span model of a rectangular planform wing with the NACA 0015 section showed no evidence of separation cells regardless of angle of attack. Second, a three-dimensional numerical simulation[10] of the water-tunnel experiments, assuming laminar flow, also failed to reproduce the separation cells. Very recently, a three-dimensional numerical simulation was performed using the same wing geometry at a much higher Reynolds number ($>1 \times 10^6$) and including turbulent kinetic energy production. Preliminary results indicate that the characteristic multiple separation cell pattern can be reproduced numerically on rectangular wings of sufficiently high aspect ratio if turbulent conditions are assumed. In addition, the calculations to date have been steady state, supporting the observation that unsteady shear layer phenomena are not required for stall cell formation.

The far wake, as determined by measurement of pressure fluctuations approximately 6 chords downstream of the model, is subject to an instability consistent with a von Kármán vortex street in both the shallow and deep stall regimes, independent of the state of the separated region in the vicinity of the model. Although the large-amplitude, low-frequency fluctuations recorded on the model surface in the shallow stall regime may persist some distance into the wake, the structures responsible for the pressure fluctuations recorded in the near and far wake regions are essentially independent at all model incidence angles.

The low-frequency fluctuations recorded on the model surface, which may correspond to the shear layer flapping noted by Zaman et al.,[4] occur within a restricted range of incidence angles and appear to result from a fundamental instability of the (turbulent) separated flow, distinct from the von Kármán vortex street, which is subject to forcing at externally imposed frequencies.

Conclusions

Spanwise cellular patterns in the poststall flow over rectangular wings have been observed in association with large-amplitude surface pressure fluctuations that occur with frequencies much lower than those anticipated for bluff body shedding. Analysis of the unsteady pressure histories suggests that although both phenomena may be related to instabilities in the separated shear layer, there is no simple connection between the two. The combined results of these experiments and the numerical simulation of Ref. 10 suggest that the interaction between the wing surface and the leading-edge (separated) and trailing-edge shear layers may be responsible for the low-frequency fluctuations. In addition, the apparent lack of discrete structures resulting from deformation of the separated shear layer precludes subsequent deformation of these spanwise vortices as the cause of cellular separation. In the wake, instability of the evolving wake profile results in pressure fluctuations consistent with a von Kármán vortex street. The near- and far-wake regions, distinguished by the frequency content of the dominant pressure fluctuations, appear to be independent, implying that the von Kármán vortex street does not substantially influence wing surface pressures.

Acknowledgments

This work was funded through NASA Ames Research Center Joint Research Consortium Agreement NCA2-786, with James Ross as Project Monitor.

References

[1]Ericsson, L. E., "Effect of Karman Vortex Shedding on Airfoil Flutter," AIAA Paper 86-1789, June 1986.

[2]Armstrong, E. K., and Stevenson, M. A., "Some Practical Aspects of Compressor Blade Vibration," *Journal of the Royal Aeronautical Society*, Vol. 64, March 1960, pp. 117–130.

[3]Baker, J. E., "The Effects of Various Parameters, Including Mach Number, on Propeller Blade Flutter with Emphasis on Stall Flutter," NACA TN-3357, Jan. 1955.

[4]Zaman, K. M. B. Q., McKinzie, D. J., and Rumsey, C. L., "A Natural Low-Frequency Oscillation of the Flow over an Airfoil Near Stalling Conditions," *Journal of Fluid Mechanics*, Vol. 202, May 1989, pp. 403–442.

[5]Moss, N. J., "Measurement of Aerofoil Unsteady Stall Properties with Acoustic Flow Control," *Journal of Sound and Vibration*, Vol. 65, No. 4, 1979, pp. 505–520.

[6]Gregory, N., Quincy, V. G., O'Reilly, C. L., and Hall, D. J., "Progress Report on Observations of Three Dimensional Flow Patterns Obtained During Stall Development on Aerofoils, and on the Problem of Measuring Two-Dimensional Characteristics," Fluid Motion Sub-Committee, Aeronautical Research Council, 31 702, NPL Aero Rept. 1309, Teddington, Middlesex, England, UK, Jan. 1970.

[7]Winkelmann, A. E., and Barlow, J. B., "Flowfield Model for a Rectangular Planform Wing Beyond Stall," *AIAA Journal*, Vol. 18, No. 8, 1980, pp. 1006–1008.

[8]Weihs, D., and Katz, J., "Cellular Patterns in Poststall Flow over Unswept Wings," *AIAA Journal*, Vol. 21, No. 12, 1983, pp. 1757, 1758.

[9]Crow, S. C., "Stability Theory for a Pair of Trailing Vortices," *AIAA Journal*, Vol. 8, No. 12, 1970, pp. 2172–2179.

[10]Yon, S. A., "Coherent Structures in the Wake of a Stalled Rectangular Wing," Ph.D. Thesis, Dept. of Applied Mechanics, Univ. of California, San Diego, CA, and College of Engineering, San Diego State Univ., San Diego, CA, 1995.

[11]Katz, J., and Plotkin, A., *Low Speed Aerodynamics, From Wing Theory to Panel Methods*, McGraw–Hill, New York, 1991, Chap. 11.

[12]Gharib, M., and Williams-Stuber, K., "Experiments on the Forced Wake of an Airfoil," *Journal of Fluid Mechanics*, Vol. 208, Nov. 1989, pp. 225–255.

[13]Cimbala, J., Nagib, H., and Roshko, A., "Wake Instability Leading to New Large Scale Structures Downstream of Bluff Bodies," *Bulletin of the American Physical Society*, Vol. 26, Nov. 1981, p. 1256.

[14]Katz, J., Yon, S., and Rogers, S. E., "Impulsive Start of a Symmetric Airfoil at High Angle of Attack," *AIAA Journal*, Vol. 34, No. 2, 1996, pp. 225–230.

R. W. Wlezien
Associate Editor